



HAL
open science

Construction of a spanning tree for high-order edge elements

Eduardo de Los Santos, Ana Maria Alonso Rodríguez, Francesca Rapetti

► **To cite this version:**

Eduardo de Los Santos, Ana Maria Alonso Rodríguez, Francesca Rapetti. Construction of a spanning tree for high-order edge elements. *International Journal of Numerical Modelling: Electronic Networks, Devices and Fields*, 2022. hal-03426095v1

HAL Id: hal-03426095

<https://hal.science/hal-03426095v1>

Submitted on 12 Nov 2021 (v1), last revised 18 Dec 2023 (v2)

HAL is a multi-disciplinary open access archive for the deposit and dissemination of scientific research documents, whether they are published or not. The documents may come from teaching and research institutions in France or abroad, or from public or private research centers.

L'archive ouverte pluridisciplinaire **HAL**, est destinée au dépôt et à la diffusion de documents scientifiques de niveau recherche, publiés ou non, émanant des établissements d'enseignement et de recherche français ou étrangers, des laboratoires publics ou privés.

ARTICLE TYPE

Construction of a spanning tree for high-order edge elements

Eduardo De Los Santos¹ | Ana Maria Alonso Rodríguez¹ | Francesca Rapetti²¹Dip. di Matematica, Univ. di Trento, Povo, Trento, Italy²Dept. de Mathématiques., Univ. Côte d'Azur, Nice, France**Correspondence**

*Eduardo De Los Santos Email: ea.delossantosnunez@unitn.it

Present Address

Dip. di Matematica, Univ. di Trento, via Sommarive 14, I-38123 Povo, Trento

Summary

The well-known tree-cotree gauging method for low-order edge finite elements is extended to high-order approximations within the first family of Nédélec finite element spaces. The key point in this method is the identification of degrees of freedom for edge and nodal finite element spaces such that the matrix of the gradient operator is the transposed of the all-node incidence matrix of a directed graph. This is straightforward for low-order finite elements and it can be proved that it is still possible in the high-order case using either moments or weights as degrees of freedom. In the case of weights, the geometrical realization of the graph associated with the gradient operator is very natural. We recall in details the definition of weights and present an algorithm for the construction of a spanning tree of this graph. The starting point of the algorithm is a spanning tree of the graph given by vertices and edges of the mesh (the so-called global spanning tree, that is the one used in the low-order case). This global step, interpreted in the high-order sense, is enriched locally, with a loop over the elements of the mesh, with arcs corresponding to edge, face and volume degrees of freedom required in the high-order case.

KEYWORDS:

High-order edge elements, tree-cotree gauge, small simplices' graph, incidence matrix.

1 | INTRODUCTION

The aim of this work is to present the construction of a spanning tree of the graph associated with the degrees of freedom of high-order nodal and edge finite elements to extend the well-known tree-cotree gauging method. In the high-order case, the difficulty is that we do not have a one-to-one correspondence between field unknowns and mesh edges, as we have more unknowns in each mesh tetrahedron. Using the weights^{1,2,3} as degrees of freedom (dofs) for high-order edge finite elements, the graph can be thought on a particular refinement associated with the *principal lattice* of the elements of the initial mesh. The small tetrahedra generated by this refinement that are affine contraction of those of the initial mesh are called small elements. They are not constructed actually, but they allow for a geometrical localization of dofs for high-order edge finite elements and thus for a visualization of the graph for any polynomial degree.

Whitney edge elements⁴ are widely recognized as a useful tool for computational electromagnetism⁵. They offer a simple construction of polynomial discrete differential forms on simplicial complexes^{6,7}. Their associated dofs have a very clear physical meaning (circulation of the approximated field on the edges of the element)⁴. Because they model the curl kernel well, the matrix associated with the curl-curl operator is singular, and this singularity is related to the graph whose *geometrical realization* is the finite element mesh, i.e., the arcs of the graph are the edges of the mesh and the nodes of the graph are the vertices of the mesh. Specifically, when the domain is simply connected, a tree-cotree decomposition of the arcs of this graph, was shown to classify dofs into dependent and independent ones for the curl operator⁸ in the sense that a vector potential with fixed values of its independent dofs (identified by means of the tree) is unique^{9,10}. This fact was successfully applied in a three-dimensional magnetostatic problem¹¹ and also in a nonlinear eddy current problem¹². Tree-cotree decomposition of the graph is also useful to constraint the vector potential (without fixing to zero the independent dofs), this can be understood as the discrete version of the classical Coulomb gauge¹³. In

⁰Abbreviations: Spanning tree for high-order edge elements

non simply-connected domains, the curl kernel is augmented with some elements that are not gradient of a scalar function. Hence, the spanning tree is suitably extended into a *belted spanning tree*⁵.

The high-order case is more involved. In the development of high-order extensions of Whitney edge elements, the classical approach^{14,15,16} introduces moments to define the needed dofs. Such a construction includes dofs associated with faces and tetrahedra that can not be interpreted as field circulations along edges and consequently it does not allow for an immediate geometrical realization of the graph. The approach proposed in^{1,17,18} generalizes to higher orders the methodology of Whitney: if one finds a way to represent a manifold of dimension k by a k -chain (i.e., formal sum of mesh simplices of dimension k) then by duality one knows how to represent a field by a finite weighted sum of basis fields (the Whitney forms).

In this work, we follow this approach that yields new dofs for high-order approximations, the so-called *weights*^{3,19,20}. In the case of nodal elements, they are the classical functionals that associate with a function its values at the small vertices that are the nodes of the principal lattices of the mesh elements. In the case of edge elements, they are functionals that associate with a field its circulations along the *small edges*, that are the edges of the small tetrahedra^{2,18}. These weights are relevant, since they pop up naturally when we generalize Whitney construction to the high-order case. Note that, each small edge can be localized either (i) on an edge of the mesh, or (ii) at the interior of a face of the mesh or (iii) at the interior of an element of the mesh. The small edges for high-order extensions of Whitney 1-forms are always linking adjacent points of the principal lattice of the same order. They have the same orientation and are parallel to edges of the mesh. When dofs are weights, the matrix representative of the gradient is an incidence matrix (between small edges and small vertices) for any polynomial degree²¹. On the other hand, the duality property between unisolvent dofs (circulations on small edges) and generators of the discrete finite element space is lost in the high-order case if all the edges of the small tetrahedra are considered. Duality is recovered by choosing an appropriate subset²² of the small edges. The resulting graph, with the principal lattices of the mesh elements as nodes and this subset of small edges as arcs, is an oriented connected graph. Let us consider the canonical basis of the nodal and edge finite element spaces for the weights supported on the nodes and arcs of this graph respectively. In this context, we are interested in the matrix that represents the gradient as a linear operator between finite dimensional spaces. This means, the matrix that computes the circulations along the small edges of a field that is the gradient of a nodal finite element function knowing the values of this function at the nodes of the principal lattices of the mesh elements. It is easy to see that this matrix is the transposed of the all-node incidence matrix of the graph. In the simply connected case the gradients of the nodal finite elements fill-in the kernel of the curl operator acting on edge finite element functions. Then the selection of a spanning tree of this graph is a useful tool for the identification of high-order potentials²⁵ or for the tree-cotree gauge within high-order approximations. In this contribution we propose an efficient algorithm for the construction of a spanning tree of this graph.

The outline of this work is as follows. In Section 2 we introduce the fundamental notion of small simplices. In Section 3 we explain how to use this notion to define basis and dofs for high-order Whitney finite elements and we introduce the high-order graph induced by the supports of these dofs. We then relate this graph with the matrix that represents the gradient operator on the canonical bases. Finally in Section 4 we present the algorithm for the construction of the spanning tree of the high-order graph and some considerations on its particularities.

2 | SMALL SIMPLICES

Let $\mathcal{T} = (V, E, F, T)$ be a tetrahedral mesh of the polyhedral domain Ω of \mathbb{R}^3 , where V is the set of vertices, E is the set of edges, F is the set of faces, and T is the set of tetrahedra of \mathcal{T} . Let $\Delta_d(\mathcal{T})$ denote the set of d -simplices of the mesh, for $d \in \{0, 1, 2, 3\}$, thus $\Delta_0(\mathcal{T}) = V$, $\Delta_1(\mathcal{T}) = E$, $\Delta_2(\mathcal{T}) = F$, and $\Delta_3(\mathcal{T}) = T$. Let us fix an orientation on each edge, face, and tetrahedron of \mathcal{T} . This can be done by choosing a total ordering of the vertices in $V = \{\mathbf{v}_i\}_{i=1}^{N_V}$, where \mathbf{v}_i denotes the (Cartesian) coordinates of the node n_i in \mathbb{R}^3 , and by associating with each d -simplex of the mesh, $S \in \Delta_d(\mathcal{T})$, an increasing function $m_S : \{0, 1, \dots, d\} \rightarrow \{1, \dots, N_V\}$. The oriented d -simplex S is hence given by $S = [\mathbf{v}_{m_S(0)}, \dots, \mathbf{v}_{m_S(d)}]$.

For $S \in \Delta_d(\mathcal{T})$, we denote by $\Delta_\ell(S)$ the set of ℓ -simplices contained in S , for $\ell \in \{0, \dots, d\}$. If $\Sigma \in \Delta_\ell(S)$ with $\ell \in \{0, \dots, d-1\}$, then there exists a unique increasing map $m_\Sigma^S : \{0, \dots, \ell\} \rightarrow \{0, \dots, d\}$ such that, for each $i \in \{0, \dots, \ell\}$, $m_\Sigma(i) = m_S(m_\Sigma^S(i))$.

For $r, d \in \mathbb{N}_0 := \mathbb{N} \cup \{0\}$, let us set

$$\mathcal{I}(d+1, r) := \{\boldsymbol{\eta} = (\eta_0, \dots, \eta_d) \in \mathbb{N}_0^{d+1} : |\boldsymbol{\eta}| = r\},$$

being $|\boldsymbol{\eta}| := \sum_{i=0}^d \eta_i$. The cardinality of $\mathcal{I}(d+1, r)$ is equal to $\binom{r+d}{d} = \frac{(r+d)!}{r!d!}$.

For a point \mathbf{x} in a d -simplex $S \in \Delta_d(\mathcal{T})$ (with $d \in \{1, 2, 3\}$), we denote by $\boldsymbol{\lambda}_S(\mathbf{x}) = (\lambda_{m_S(0)}^S(\mathbf{x}), \dots, \lambda_{m_S(d)}^S(\mathbf{x}))$ the vector of its barycentric coordinates with respect to the vertices $\{\mathbf{v}_{m_S(0)}, \dots, \mathbf{v}_{m_S(d)}\}$ of S . Each function $\lambda_{m_S(\ell)}^S : S \rightarrow \mathbb{R}$ satisfies the property $\lambda_{m_S(\ell)}^S(\mathbf{v}_{m_S(j)}) = \delta_{j,\ell}$, with $\ell, j \in \{0, \dots, d\}$. The functions $\lambda_{m_S(\ell)}^S$ are positive at the interior of S , and non negative on S . The barycentric coordinates also satisfy the properties of representation of points and partition of unity, namely

$$\mathbf{x} = \sum_{j=0}^d \lambda_{m_S(j)}^S(\mathbf{x}) \mathbf{v}_{m_S(j)} \quad \text{and} \quad \sum_{j=0}^d \lambda_{m_S(j)}^S(\mathbf{x}) = 1.$$

Let $t \in T$, for each $i \in \{1, \dots, n_V\}$ we denote $\lambda_i : \bar{\Omega} \rightarrow \mathbb{R}$

$$\lambda_i : \mathbf{x} \mapsto \lambda_i(\mathbf{x}) = \begin{cases} \lambda_{m_t(\ell)}^t(\mathbf{x}) & \text{if } \mathbf{x} \in t \text{ and } i = m_t(\ell) \text{ with } \ell \in \{0, \dots, 3\} \\ 0 & \text{otherwise.} \end{cases}$$

The set of real valued polynomials defined on S of degree less than or equal to r is denoted by $\mathcal{P}_r(S)$ and the subspace of $\mathcal{P}_r(S)$ of homogeneous polynomials of degree r is denoted by $\tilde{\mathcal{P}}_r(S)$. We have $\dim \mathcal{P}_r(S) = \binom{r+d}{d}$ and $\dim \tilde{\mathcal{P}}_r(S) = \binom{r+d-1}{d}$. When S is reduced to a single point, then $\mathcal{P}_r(S) = \mathbb{R}$ for all $r \geq 0$. For any S , if $r < 0$, then $\mathcal{P}_r(S) = \{0\}$. It is known that the barycentric coordinate functions $\lambda_{m_S(i)}^S$ constitute a basis for $\mathcal{P}_1(S)$. Homogeneous polynomials of degree r in the $d+1$ barycentric coordinates are in 1-to-1 correspondence with polynomials of degree $\leq r$ in the d Cartesian coordinates. For this reason, we have that $\mathcal{P}_r(S) = \text{Span}_{\alpha \in \mathcal{I}(d+1, r)} \{\lambda_S^\alpha\}$. Given S , we define the continuous function

$$\lambda_S^\alpha : \mathbf{x} \mapsto \lambda_S^\alpha(\mathbf{x}) = \begin{cases} \prod_{j=0}^d [\lambda_{m_S(j)}^S(\mathbf{x})]^{\alpha_j} & \text{if } \alpha \in \mathcal{I}(d+1, r) \\ 0 & \text{otherwise.} \end{cases}$$

Definition 1 (Principal lattice of order $r+1$). Given $S = [m_S(0), \dots, m_S(d)]$ and an integer $r \geq 0$, the principal lattice of order $r+1$ in the d -simplex S is the set of points

$$L_{r+1}(S) = \left\{ \mathbf{x} \in S : \lambda_{m_S(j)}^S \in \left\{ 0, \frac{1}{r+1}, \frac{2}{r+1}, \dots, \frac{r}{r+1}, 1 \right\}, 0 \leq j \leq d \right\}.$$

Equivalently,

$$L_{r+1}(S) = \left\{ \mathbf{x} \in S : \mathbf{x} = \frac{1}{|\beta|} \sum_{j=0}^d \beta_j \mathbf{v}_{m_S(j)}, \forall \beta \in \mathcal{I}(d+1, r+1) \right\}.$$

Definition 2 (Small k -simplex). Let $S \in \Delta_d(\mathcal{T})$ and $\alpha \in \mathcal{I}(d+1, r)$, for an integer $r \geq 0$. The small d -simplex $\{\alpha, S\}$ is the d -simplex with barycenter at the point of Cartesian coordinates

$$\frac{1}{r+1} \sum_{j=0}^d \left[\left(\frac{1}{d+1} + \alpha_j \right) \mathbf{v}_{m_S(j)} \right]$$

and $1/(r+1)$ -homothetic to S . For any $\Sigma \in \Delta_\ell(S)$, the small ℓ -simplex $\{\alpha, \Sigma\}$ is the ℓ -simplex which is parallel, equally oriented to Σ and belongs to the small d -simplex $\{\alpha, S\}$.

The small simplices do not pave the d -simplex S . The holes left are not homothetic to S but the algorithm we present does not see the holes.

In Figure 1 is presented a triangle $f = [n_0, n_1, n_2]$ together with its principal lattice $L_{r+1}(f)$ for $r = 2$. In grey we have the corresponding family of small simplices. In this case, the holes (in white) are 3 reversed triangles. In Figure 2 we have the small simplices associated with the principal lattice $L_3(t)$ in a tetrahedron $t = [n_0, n_1, n_2, n_3]$. The resulting decomposition of t includes 10 small tetrahedra, and 5 holes (4 octahedra and 1 reversed tetrahedron). On each face of the boundary of t we can see 6 small-faces and 3 holes. Note that each edge of t is decomposed in 3 small edges.

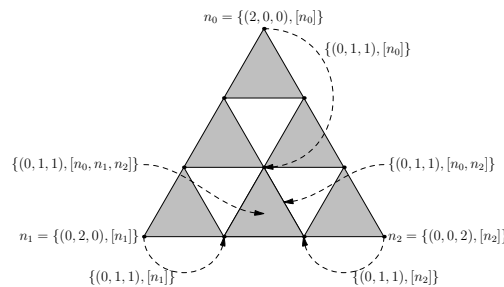


FIGURE 1 Principal lattice $L_3(f)$ in the face $f = [n_0, n_1, n_2]$, with the visualization of all the small simplices. The label of the small-simplex $\{(0, 1, 1), [n_0, n_1, n_2]\}$ and of some of its sub-simplices are indicated for illustration.

The small simplices are of key importance in the generalization of Whitney finite elements to higher order. Indeed, they allow to make a list of the generators of any polynomial degree of the finite element spaces and constitute the support of new dofs, the weights, for the representation of fields in these discrete spaces (together with a direct geometrical visualization of the tree-cotree structure that we discuss in the last part of the present work).

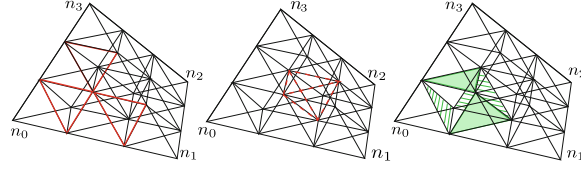


FIGURE 2 (Taken from reference [25]). Principal lattice $L_3(t)$ in the tetrahedron $t = [n_0, n_1, n_2, n_3]$, with the visualization of all the small simplices. Each face of the boundary of t is decomposed in 6 small-faces and 3 reversed triangles (highlighted on the left with red solid lines). The decomposition of t includes 10 small tetrahedra, 1 reversed tetrahedron (highlighted at the center with red dashed lines) and 4 octahedra (one is highlighted on the right in green).

3 | HIGH-ORDER WHITNEY EDGE ELEMENTS AND THE HIGH-ORDER GRAPH

For a more compact presentation, we rely on the notation of the finite element exterior calculus. It is well known (see^{23,20}) that the proxy fields of the space of trimmed polynomial differential forms usually denoted $\mathcal{P}_{r+1}^- \Lambda^k(\mathcal{T})$ are the finite element space of Lagrange of degree $r + 1 \geq 1$ if $k = 0$, the first family of Nédélec finite elements of order $r + 1$ conforming in $H(\text{curl}; \Omega)$ if $k = 1$, the first family of Nédélec finite elements of order $r + 1$ conforming in $H(\text{div}; \Omega)$ if $k = 2$, and discontinuous elements of degree $\leq r$ if $k = 3$. Let d be the exterior derivative for differential k -forms for $k < d$.

Definition 3 (Whitney k -forms). In a tetrahedron t , Whitney k -forms associated with $S \in \Delta_k(t)$ are the fields

$$w_S = \begin{cases} \lambda_{m_S(0)}, & \text{with } k = 0, S = [n_{m_S(0)}], \\ \sum_{j=0}^k (-1)^j \lambda_{m_S(j)} d w_{S-[n_{m_S(j)}]}, & \text{with } k > 0, S = [n_{m_S(0)}, \dots, n_{m_S(k)}]. \end{cases}$$

In particular, for $k = 1$ the exterior derivative d corresponds to the gradient operator and Definition 3 yields

$$w_S = \lambda_{m_S(0)} \text{grad } \lambda_{m_S(1)} - \lambda_{m_S(1)} \text{grad } \lambda_{m_S(0)}.$$

Whitney k -forms of higher degree in each tetrahedron t can be associated with the principal lattice in t as recalled in the next Definition.

Definition 4 (Higher-order Whitney k -forms). In a tetrahedron t , Whitney k -forms of higher polynomial degree are the fields

$$w_s = \lambda_t^\alpha w_S,$$

for all the small k -simplices $s := \{\alpha, S\}$, with $\alpha \in \mathcal{I}(4, r)$ for $r > 0$, and $S \in \Delta_k(t)$, being w_S is the Whitney k -form associated with S . The space of high-order Whitney k -forms in t is

$$\mathcal{P}_{r+1}^- \Lambda^k(t) = \text{Span} \{w_s : s = \{\alpha, S\}, \alpha \in \mathcal{I}(4, r), S \in \Delta_k(t)\}.$$

Fields in $\mathcal{P}_{r+1}^- \Lambda^k(t)$ are defined as products between a field in $\mathcal{P}_1^- \Lambda^k(t)$ and the continuous function λ_t^α , $\alpha \in \mathcal{I}(4, r)$. Therefore, fields in $\mathcal{P}_{r+1}^- \Lambda^k(t)$ enjoy the same conformity properties as those in $\mathcal{P}_1^- \Lambda^k(t)$ ³.

Definition 5 (Weights on small k -simplices). For a polynomial k -form $u \in \mathcal{P}_{r+1}^- \Lambda^k(t)$, with $0 \leq k \leq 3$ and $r \geq 0$, the weights are the reals

$$\int_{\{\alpha, S\}} u, \tag{1}$$

for all the small k -simplices $\{\alpha, S\}$, with $\alpha \in \mathcal{I}(4, r)$ and $S \in \Delta_k(t)$.

The weights of a high-order Whitney k -form $u \in \mathcal{P}_{r+1}^- \Lambda^k(t)$ along all the small k -simplices $\{\alpha, S\}$ of a mesh \mathcal{T} are *unisolvent*²⁴, Proposition 3.14, namely if $u \in \mathcal{P}_{r+1}^- \Lambda^k(t)$ is such that $\int_{\{\alpha, S\}} u = 0$ for all the small k -simplices $s = \{\alpha, S\}$ then $u = 0$. The small k -simplices can thus support the dofs for fields $u \in \mathcal{P}_{r+1}^- \Lambda^k(t)$. Since the result on unisolvence holds true also by replacing t with $\Sigma \in \Delta_\ell(t)$ (with $k \leq \ell < 3$), then the respective trace of u over any $\Sigma \in \Delta_\ell(t)$ (trace that lives in $\mathcal{P}_{r+1}^- \Lambda^k(\Sigma)$) is uniquely determined by the weights localized on small k -simplices in Σ . We thus can use the weights on the small k -simplex $\{\alpha, S\}$ as dofs for the fields in the finite element space $\mathcal{P}_{r+1}^- \Lambda^k(\mathcal{T})$, being aware that their number is greater than the dimension of the space.

The weights given in Definition 5 have a meaning as cochains and this relates directly the matrix describing the exterior derivative with the matrix of the boundary operator. The key point is the Stokes theorem $\int_C du = \int_{\partial C} u$, where u is a $(k - 1)$ -form and C a k -chain. More precisely,

if $u \in \mathcal{P}_{r+1}^- \Lambda^k(\mathcal{T})$ then $du \in \mathcal{P}_{r+1}^- \Lambda^{k+1}(\mathcal{T})$ and

$$\int_{\{\alpha, S\}} du = \int_{\partial\{\alpha, S\}} u = \sum_{\{\beta, \Sigma\}} \mathbf{B}_{\{\alpha, S\}, \{\beta, \Sigma\}} \int_{\{\beta, \Sigma\}} u, \quad (2)$$

being \mathbf{B} the boundary matrix with as many rows as small k -simplices, and as many columns as small $(k-1)$ -simplices. The small k -simplex $\{\alpha, S\}$ inherits the orientation of the k -simplex S , so the coefficient $\mathbf{B}_{\{\alpha, S\}, \{\beta, \Sigma\}}$ is equal to the coefficient $\mathbf{B}_{S, \Sigma}$ of the boundary of the simplex S if $\beta = \alpha$ and zero otherwise. Therefore, $\mathbf{B}_{S, \Sigma}$ is 1 or -1 depending of whether the orientation of Σ matches or not with the orientation induced by that of the k -simplex S on its $(k-1)$ -face Σ , and $\mathbf{B}_{S, \Sigma}$ is zero when Σ is not part of the boundary of S . This fact is straightforward if $\dim(\Sigma) > 0$, but also when $\dim(\Sigma) = 0$ ²¹. For $k = 1$, note that the matrix $\mathbf{B}_{\{\alpha, S\}, \{\beta, \Sigma\}}$ is an incidence matrix between small edges and small vertices; moreover, it is an all-node incidence matrix of a (non connected) graph, whose geometrical realization is shown on the right of Figure 3.

Remark: For $k = 1$, in order to have \mathbf{B} an incidence matrix between small edges and small vertices, some points in the principal lattice have different labels. The point $\frac{1}{|\eta|} \sum_{j=0}^3 \left[\left[\frac{1}{4} + \eta_j \right] \mathbf{v}_{m_t(j)} \right] \in L_3(t)$, with $\eta = (2, 0, 1, 0)$ has a label as the small vertex $\{(2, 0, 0, 0), [n_2]\}$ (the brown point in the fragmented visualization) and also as the small vertex $\{(1, 0, 1, 0), [n_0]\}$ (the black point in the fragmented visualization). However, the 0-forms associated with the different labels are the same. Indeed, $\{(2, 0, 0, 0), [n_2]\}$ corresponds with the 0-form $\lambda_{m_t(0)}^2 w_{n_2} = \lambda_{n_0}^2 \lambda_{n_2}$ and $\{(1, 0, 1, 0), [n_0]\}$ with the 0-form $\lambda_{m_t(0)} \lambda_{m_t(2)} w_{n_0} = \lambda_{n_0} \lambda_{n_2} \lambda_{n_0} = \lambda_{n_0}^2 \lambda_{n_2}$, and we can see that "both" 0-forms are actually the same.

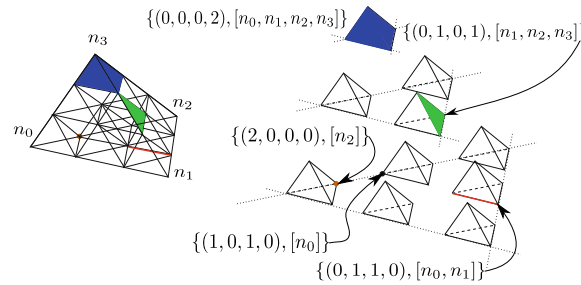


FIGURE 3 (Taken from reference [21]). Visualization (on the left) of all the small simplices associated with the principal lattice $L_3(t)$ in the tetrahedron $t = [n_0, n_1, n_2, n_3]$. The same set of small simplices in a fragmented visualization (on the right), a small tetrahedron in blue, a small face in green, a small edge in red and small vertex in brown and also in black (the different labels for the same point in the principal lattice $L_3(t)$).

We say that a set of unisolvent degrees of freedom for high-order Whitney edge finite elements is minimal if its cardinality is equal to the dimension of the finite element space. In order to use a set of minimal unisolvent degrees of freedom for high-order Whitney edge finite elements we have to disregard some small edges. In fact it can be proved²² that to be unisolvent it is enough to consider on each face small edges parallel to two of the three edges of the face and on each tetrahedra small edges parallel to three of the six edges of the tetrahedra. Proceeding in this way the corresponding set of weights is unisolvent and minimal.

We use the term *active* to indicate all the small k -simplices such that $\lambda_\ell^\alpha w_S$ belongs to a basis of $\mathcal{P}_{r+1}^- \Lambda^k(\mathcal{T})$. The dimension of the space $\mathcal{P}_{r+1}^- \Lambda^k(\mathcal{T})$ coincides with the number of *active small k -simplices* in the mesh \mathcal{T} ²⁵. We recall the following result^{26, Proposition 6.4}:

Proposition 1 (A basis of $\mathcal{P}_{r+1}^- \Lambda^k(t)$). The set

$$\{\lambda_\ell^\alpha w_S : \alpha \in \mathcal{I}(4, r), S \in \Delta_k(t) \text{ and } \alpha_j = 0 \text{ if } j < m_S^t(0)\}$$

is a basis of $\mathcal{P}_{r+1}^- \Lambda^k(t)$.

A possible rule for selecting the active small vertices $\{\alpha, [n_i]\}$ and set of small edges $\{\alpha, [n_{m_e(0)}, n_{m_e(1)}]\}$ that induces minimal and unisolvent weights is the same given in Proposition 1 to select a basis of $\mathcal{P}_{r+1}^- \Lambda^k(t)$.

We denote by d_L and d_N the dimension of $\mathcal{P}_{r+1}^- \Lambda^0(\mathcal{T})$ and $\mathcal{P}_{r+1}^- \Lambda^1(\mathcal{T})$, respectively. We consider the graph with nodes the set $\{\mathbf{q}_\ell\}_{\ell=1}^{d_L}$ of active small vertices (the points of the principal lattices of the mesh elements) and arcs the set $\{\mathbf{e}_m\}_{m=1}^{d_N}$ of active small edges. Let $\{\phi_{h,i}\}_{i=1}^{d_L}$ and $\{\omega_{h,j}\}_{j=1}^{d_N}$ be the canonical bases of the nodal and edge finite element spaces for the weights supported on the nodes and arcs of this graph respectively. This means that $\phi_{h,i}(\mathbf{q}_\ell) = \delta_{i,\ell}$ and $\int_{\mathbf{e}_m} \omega_{h,j} = \delta_{j,m}$ where $\delta_{\cdot,\cdot}$ is the Kronecker delta. For each active small edge \mathbf{e}_m we denote $\mathbf{q}_{m,ini}$ and $\mathbf{q}_{m,fin}$ its initial and final small nodes respectively. It is well known that if the function ψ_h belongs to the space of nodal Lagrangian finite elements of degree $r+1$ then $\text{grad } \psi_h$ belongs to the first family of Nédélec finite elements of degree $r+1$, and clearly $\int_{\mathbf{e}_m} \text{grad } \psi_h = \psi_h(\mathbf{q}_{m,fin}) - \psi_h(\mathbf{q}_{m,ini})$. Therefore when using these canonical bases, the matrix that gives the circulations along the small edges of the gradient

of a nodal finite element function knowing the values of this function at the nodes principal lattices of the mesh elements is the transposed of the all-node incidence matrix of the graph with nodes the small vertices and arcs the active small edges.

Its geometrical realization in a tetrahedron is shown (in a fragmented version for a friendly visualization) in Figure 4. It is worthwhile to mention that the set of *active weights* is proved to be unisolvent in²². The structure shown in the Figure 4 has to be replicated on each tetrahedron $t \in T$. After this operation, we obtain the high-order graph, \mathcal{G}_{ho} , over which we can construct the high-order spanning-tree, \mathcal{S}_{ho} .

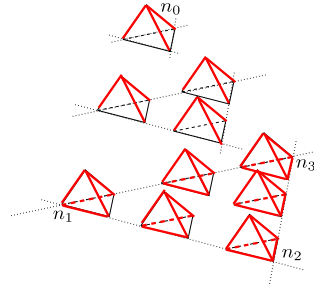


FIGURE 4 (Taken from reference [25]). A fragmented visualization of the geometrical realization of the connected graph in a tetrahedron with the active small edges (in red) as arcs and active small vertices as nodes.

4 | ALGORITHM FOR THE CONSTRUCTION OF THE SPANNING-TREE (THE HIGH-ORDER CASE)

Thanks to additional information given by the geometrical localization of the connected graph formed by the active small vertices and the active small edges shown in 4, we propose in the Algorithm 2 a suitable set of rules to construct a spanning-tree in the referred graph for each tetrahedron; then we use this set of rules to construct a convenient *global* spanning-tree \mathcal{S}_{ho} , giving in this way a classification rule in the set of active small-edges of the mesh \mathcal{T} . The *global* algorithm has as input the connected and directed graph (V, E) , and also a spanning-tree \mathcal{S} of this graph. The spanning tree \mathcal{S} can be obtained by applying algorithms such as the *Breadth-First search* or *Depth-First search* in the graph \mathcal{G} . The arcs of \mathcal{G} that are not in the spanning tree compose the cotree \mathcal{S}^c . The global algorithm starts reading the arcs of the given spanning-tree \mathcal{S} (Algorithm 1).

Algorithm 1 Initialization of Algorithm 2

Require: The mesh $\mathcal{T} = (V, E, F, T)$, and a spanning-tree \mathcal{S} of the graph (V, E) .

```

1: procedure Initialization( $\mathcal{S}, E, F$ )
2:   loop over the edges  $e \in E$ 
3:     tree-flag( $e$ )  $\leftarrow$  false.
4:     visited-edge-flag( $e$ )  $\leftarrow$  false.
5:     if  $e \in \mathcal{S}$  then
6:       tree-flag( $e$ )  $\leftarrow$  true. ▷ Reading the spanning-tree  $\mathcal{S}$ 
7:     end if
8:   end loop
9:   loop over the faces  $f \in F$ 
10:    visited-face-flag( $f$ )  $\leftarrow$  false.
11:  end loop
12: end procedure

```

In Algorithm 1 the information on \mathcal{S} is saved by mean of a flag associated with each edge of the mesh (if an edge is part of the spanning-tree \mathcal{S} , the flag is set to **true**, otherwise is set to **false**); when the algorithm is initialised, the flag associated with each face is also set to **false** (we use this flag to control the previously visited face in the loop over all elements of the mesh).

The information saved in the flags is used within a loop over all the tetrahedra of the mesh, where the spanning-tree \mathcal{S}_{h_o} is constructed; in each cycle of the tetrahedra loop, the previously proposed set of rules is used conveniently. The spanning-tree \mathcal{S} gives a selection criteria to put some active small edges of the global graph in the spanning-tree \mathcal{S}_{h_o} . More precisely, all the small edges on arcs of the spanning tree \mathcal{S} and all but one (in particular the last one) the small edges on arcs of the cotree \mathcal{S}^c . Then the global spanning-tree \mathcal{S}_{h_o} is further enriched with some active small edges at the interior of each face (only those faces of the tetrahedra that have not been visited previously), and finally with some active small edges at the interior of each tetrahedron. The proposed algorithm can be executed as part of pre-processing step. The algorithm requires as input \mathcal{G} , \mathcal{S} , \mathcal{G}_{h_o} , also the faces and tetrahedra of the mesh; and gives as output the enriched spanning-tree \mathcal{S}_{h_o} .

Algorithm 2 A spanning-tree of active small-edges

Ensure: A spanning-tree \mathcal{S}_{h_o} of the graph with nodes: the active small vertices; and arcs: the active small edges.

```

13: procedure Construction of  $\mathcal{S}_{h_o}(E,F,T,\text{tree-flag,visited-edge-flag,visited-face-flag})$ 
14:   loop over the tetrahedra  $t \leftarrow [n_a, n_b, n_c, n_d] \in T$ 
15:     loop over the faces  $f \leftarrow [n_i, n_j, n_k] \in \Delta_2(t)$ 
16:       if visited-face-flag( $f$ ) == false then
17:         loop over the edges  $e \leftarrow [n_p, n_q] \in \Delta_1(f)$ 
18:           if visited-edge-flag( $e$ ) == false then
19:             if tree-flag( $e$ ) == true then
20:               add to  $\mathcal{S}_{h_o}$  the small-edges  $\{\alpha, e\}, \forall \alpha \in \mathcal{I}(4, r)$  with  $\alpha_{m_{t-e}^t}(0) = 0$  and  $\alpha_{m_{t-e}^t}(1) = 0$ .       $\triangleright$  All the small-edges
                $\{\alpha, e\}$  over the edge  $e$ .
21:             else
22:               add to  $\mathcal{S}_{h_o}$  the small-edges  $\{\alpha, e\}$  corresponding to the  $r - 1$  first indices  $\alpha \in \mathcal{I}(4, r)$  with  $\alpha_{m_{t-e}^t}(0) = 0$  and
                $\alpha_{m_{t-e}^t}(1) = 0$ .       $\triangleright$  first is always intended in the reversed lexicographical order.
23:             end if
24:             visited-edge-flag( $e$ )  $\leftarrow$  true
25:           end if
26:         end loop
27:       for  $\alpha_{m_f^t(2)} \leftarrow 1$  to  $r - 1$  do
28:         add to  $\mathcal{S}_{h_o}$  the small-edges  $\{\alpha, [n_{m_f(0)}, n_{m_f(1)}]\}$  corresponding to the  $r - \alpha_{m_f^t(2)}$  first indices  $\alpha \in \mathcal{I}(4, r)$  with  $\alpha_{m_{t-f}^t}(0) =$ 
0.       $\triangleright$  Adding small-edges  $\{\alpha, [n_{m_f(0)}, n_{m_f(1)}]\}$  of the interior of  $f$  to  $\mathcal{S}_{h_o}$ .
29:       end for
30:       visited-edge-flag( $f$ )  $\leftarrow$  true
31:     end if
32:   end loop
33:   for  $\alpha_3 \leftarrow 1$  to  $r - 2$  do
34:     for  $\alpha_2 \leftarrow 1$  to  $r - (\alpha_3 + 1)$  do
35:       add to  $\mathcal{S}_{h_o}$  the small-edges  $\{\alpha, [n_{m_f(0)}, n_{m_f(1)}]\}$  corresponding to the  $r - (\alpha_2 + \alpha_3)$  first indices  $\alpha \in \mathcal{I}(4, r)$ .       $\triangleright$  Adding
       small-edges  $\{\alpha, [n_{m_t(0)}, n_{m_t(1)}]\}$  of the interior of  $t$  to  $\mathcal{S}_{h_o}$ .
36:     end for
37:   end for
38: end loop
39: end procedure

```

In Figure 5 we can see the structure of the spanning-tree \mathcal{S}_{h_o} (in green) given by the Algorithm 2, considering the case $r = 4$ in a mesh with an unique tetrahedron $t = [n_0, n_1, n_2, n_3]$; a red arc is in \mathcal{S}_{h_o} if its respective (big) edge is in the given spanning-tree \mathcal{S} , otherwise is out of \mathcal{S}_{h_o} .

In Figure 6 we can see the structure of the spanning-tree \mathcal{S}_{h_o} (in green and red) given by the Algorithm 2, considering the case $r = 4$ in a mesh with two tetrahedra. It is worth noting that the red arcs in this figure correspond to the red arcs in Figure 5 belonging to \mathcal{S}_{h_o} .

Proposition 2. If Ω is simply connected, the number $d_{\mathcal{S}_{h_o}}$ of small edges in \mathcal{S}_{h_o} is $(d_L - 1)$.

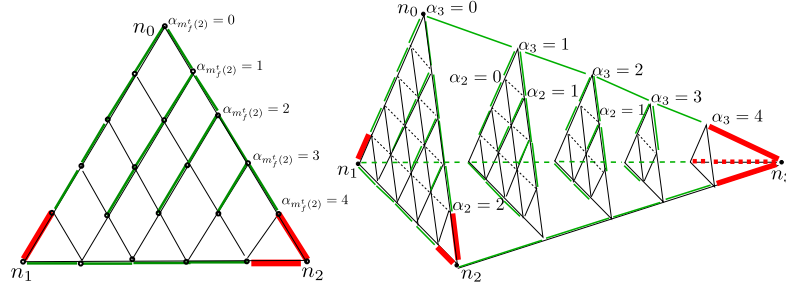


FIGURE 5 The spanning-tree S_{ho} (in green) on a tetrahedron $t = [n_0, n_1, n_2, n_3]$. On the left, the subgraph corresponding to active small-edges on the edges and in the interior of the face $f = [n_0, n_1, n_2]$, and the corresponding part of the spanning-tree S_{ho} . The red arcs belong to the spanning-tree S_{ho} , if and only if, its corresponding edge e belong to the spanning tree S . On the right, the active small-edges in the interior of t belonging to S_{ho} are visualized, (note that for a friendly visualization, some active small-edges were omitted in the figure). In this example we are considering $r = 4$.

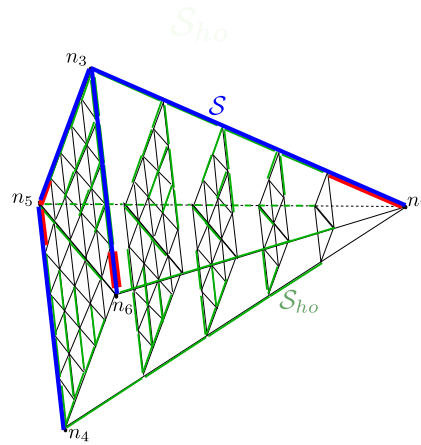


FIGURE 6 The spanning-tree S_{ho} (in green and red) on a mesh \mathcal{T} with two tetrahedra. The arcs of the spanning tree S in blue. It is worth noting that the red arcs in this figure correspond to the red arcs in Figure 5 belonging to S_{ho} . In this example we are considering $r = 4$.

Proof. For $r = 0$, the small edges coincide with the mesh edges and their number in S is $(N_V - 1)$. Moreover, $N_V = d_L$, thus the property holds true for $r = 0$.

For $r > 0$, we recall that d_L can be rewritten as

$$d_L = N_V + N_E \dim \mathcal{P}_{r-1}(e) + N_F \dim \mathcal{P}_{r-2}(f) + N_T \dim \mathcal{P}_{r-3}(t)$$

where N_V (resp., N_E , N_F , N_T) is the number of nodes (resp., edges e , faces f , tetrahedra t) in the mesh over $\bar{\Omega}$. By the proposed algorithm, the number $d_{S_{ho}}$ of active small edges in the spanning tree S_{ho} can be counted as follows

$$d_{S_{ho}} = (r+1) \#\mathcal{S} + r \#\mathcal{S}^c + N_F \sum_{q=1}^{r-1} (r-q) + N_T \sum_{q=1}^{r-2} \left[\sum_{s=1}^{r-(q+1)} r - (q+s) \right]$$

with cardinalities $\#\mathcal{S} = (N_V - 1)$ and $\#\mathcal{S}^c = N_E - (N_V - 1)$. Note that

$$\sum_{q=1}^{r-1} (r-q) = r \sum_{q=1}^{r-1} 1 - \sum_{q=1}^{r-1} q = r(r-1) - \frac{r(r-1)}{2} = \frac{r(r-1)}{2} = \dim \mathcal{P}_{r-2}(f).$$

Moreover, for the last term in $d_{S_{ho}}$ we have

$$\begin{aligned}
\sum_{q=1}^{r-2} \left[\sum_{s=1}^{r-q-1} (r-q-s) \right] &= \sum_{q=1}^{r-2} \left[(r-q) \sum_{s=1}^{r-q-1} 1 - \sum_{s=1}^{r-q-1} s \right] \\
&= \frac{1}{2} \sum_{q=1}^{r-2} [(r-q)(r-q-1)] = \frac{1}{2} \left[\sum_{q=1}^{r-2} q^2 - (2r-1) \sum_{q=1}^{r-2} q + r(r-1) \sum_{q=1}^{r-2} 1 \right] \\
&= \frac{1}{2} \left[\frac{1}{6}(r-2)(r-1)(2r-3) - \frac{1}{2}(2r-1)(r-1)(r-2) + r(r-1)(r-2) \right] \\
&= \frac{1}{2} (r-1)(r-2) \left[\frac{r}{3} - \frac{1}{2} + \frac{1}{2} - r + r \right] = \frac{1}{6} r(r-1)(r-2)
\end{aligned}$$

that is indeed $\dim \mathcal{P}_{r-3}(t)$. Summing up, we get

$$d_{S_{ho}} = N_V - 1 + N_E \dim \mathcal{P}_{r-1}(e) + N_F \dim \mathcal{P}_{r-2}(f) + N_T \dim \mathcal{P}_{r-3}(t) = d_L - 1,$$

thus the property. \square

Remark: If Ω is not simply connected, let g be the first Betti number of Ω , namely, the number of homologically independent non bounding cycles in Ω . The algorithm can be easily generalized to this case by replacing the global spanning tree, \mathcal{S} , with a global belted spanning tree, \mathcal{S}^b that has g additional arcs. Hence, the number of arc in the high-order belted spanning tree \mathcal{S}_{ho}^b is $d_{S_{ho}^b} = d_L - 1 + g$.

At a first sight, the algorithm we present seems to work on a graph with much more nodes and arcs than the one associated with the mesh used in the low-order case. In reality the high-order graph (and its incidence matrix) is not realised. We have used it only for visualization purposes. However each arc in the high-order graph corresponds with a dof (and hence with an element of the canonical basis). Therefore any action on the set of dofs can be "visualized" as an action on this fictive graph. In the algorithm we use only the low-order graph and make a local choice of dofs, that it is done once on a reference element (as in Figure 5) and applied repeatedly on the elements of the mesh. The local choice has to guarantee that the merge of all local spanning trees is a spanning tree of the (virtual) high-order graph, as illustrated in Figure 6. Algorithm 2 implements the choice illustrated in the figures.

ACKNOWLEDGMENTS

Financial disclosure

Financial support from the French MathIT program ANR-15-IDEX-01 and the Italian project PRIN 201752HKH8.

Conflict of interest

The authors declare no potential conflict of interests.

References

1. Bossavit A. Generating Whitney forms of polynomial degree one and higher. *IEEE Transactions on Magnetics* 2002; 38(2): 341-344. doi: 10.1109/20.996092
2. Rapetti F, Bossavit A. Geometrical localisation of the degrees of freedom for Whitney elements of higher order. *IET Science, Measurement & Technology* 2007; 1(1): 63-66.
3. Rapetti F, Bossavit A. Whitney forms of higher degree. *SIAM J. Numer. Anal.* 2009; 47(3): 2369-2386. doi: 10.1137/070705489
4. Bossavit A. Whitney forms: A class of finite elements for three-dimensional computations in electromagnetism. *IEE Proceedings A (Physical Science, Measurement and Instrumentation, Management and Education, Reviews)* 1988; 135(8): 493-500.
5. Bossavit A. *Computational Electromagnetism*. San Diego: Academic Press Inc. . 1998.
6. Nédélec JC. Mixed finite elements in \mathbf{R}^3 . *Numer. Math.* 1980; 35: 315-341.

7. Barton M, Cendes Z. New vector finite elements for three-dimensional magnetic field computation. *Journal of Applied Physics* 1987; 61(8): 3919–3921.
8. Albanese R, Rubinacci G. Integral formulation for 3D eddy-current computation using edge elements. *IEE Proceedings A (Physical Science, Measurement and Instrumentation, Management and Education, Reviews)* 1988; 135(7): 457–462.
9. Albanese R, Rubinacci G. Magnetostatic field computations in terms of two-component vector potentials. *Int. J. Numer. Meth. Engrng.* 1990; 29: 515–532.
10. Alonso Rodríguez A, Bertolazzi E, Ghiloni R, Valli A. Construction of a finite element basis of the first de Rham cohomology group and numerical solution of 3D magnetostatic problems. *SIAM J. Numer. Anal.* 2013; 51(4): 2380–2402. doi: 10.1137/120890648
11. Webb J, Forghani B. A single scalar potential method for 3D magnetostatics using edge elements. *IEEE Transactions on Magnetics* 1989; 25(5): 4126–4128.
12. Albanese R, Coccoresse E, Martone R, Miano G, Rubinacci G. On the numerical solution of the nonlinear three-dimensional eddy current problem. *IEEE transactions on magnetics* 1991; 27(5): 3990–3995.
13. Manges JB, Cendes ZJ. A generalized tree-cotree gauge for magnetic field computation. *IEEE Transactions on Magnetics* 1995; 31(3): 1342–1347.
14. Nédélec JC. Mixed finite elements in \mathbf{R}^3 . *Numer. Math.* 1980; 35(3): 315–341. doi: 10.1007/BF01396415
15. Nédélec JC. A new family of mixed finite elements in \mathbf{R}^3 . *Numer. Math.* 1986; 50(1): 57–81. doi: 10.1007/BF01389668
16. Monk P. *Finite element methods for Maxwell's equations*. Numerical Mathematics and Scientific Computation Oxford University Press, New York . 2003
17. Rapetti F. Comments on a High-Order Whitney Complex for Simplices. *IEEE Journal on Multiscale and Multiphysics Computational Techniques* 2019; 4: 348–355.
18. Rapetti F. High order edge elements on simplicial meshes. *M2AN Math. Model. Numer. Anal.* 2007; 41(6): 1001–1020. doi: 10.1051/m2an:2007049
19. Rapetti F. Weights computation for simplicial Whitney forms of degree one. *C. R. Math. Acad. Sci. Paris* 2005; 341(8): 519–523. doi: 10.1016/j.crma.2005.09.005
20. Alonso Rodríguez A, Rapetti F. Some remarks on spanning families and weights for high order Whitney spaces on simplices. *Comput. Math. Appl.* 2019; 78(9): 2961–2972. doi: 10.1016/j.camwa.2019.03.006
21. Alonso Rodríguez AM, Rapetti F. The discrete relations between fields and potentials with high order Whitney forms. In: . 126 of *Lect. Notes Comput. Sci. Eng.* Springer, Cham. 2019 (pp. 259–267)
22. Alonso Rodríguez A, Bruni Bruno L, Rapetti F. Minimal sets of unisolvent weights for high order Whitney forms on simplices. In: *Lect. Notes Comput. Sci. Eng.* Springer, Cham. 2020 (pp. 195–203).
23. Arnold DN, Falk RS, Winther R. Finite element exterior calculus, homological techniques, and applications. *Acta Numer.* 2006; 15: 1–155. doi: 10.1017/S0962492906210018
24. Christiansen S, Rapetti F. On high order finite element spaces of differential forms. *Mathematics of Computation* 2016; 85(298): 517–548.
25. Rapetti F, Alonso Rodríguez A. High Order Whitney Forms on Simplices and the Question of Potentials. In: *Lect. Notes Comput. Sci. Eng.* Springer, Cham. 2020 (pp. 1–16).
26. Arnold DN, Falk RS, Winther R. Geometric decompositions and local bases for spaces of finite element differential forms. *Computer Methods in Applied Mechanics and Engineering* 2009; 198(21–26): 1660–1672.